International Journal of Mechanical Sciences 144 (2018) 1–9

Contents lists available at ScienceDirect

International Journal of Mechanical Sciences

journal homepage: www.elsevier.com/locate/ijmecsci

Blast-resilience of honeycomb sandwich panels

Hamid Ebrahimi[a], Leila Keyvani Someh[b], Julian Norato[c], Ashkan Vaziri[a,*]

[a] Department of Mechanical and Industrial Engineering, Northeastern University, Boston, MA 02115 USA
[b] First Year Engineering Program, College of Engineering, Northeastern University, Boston, MA 02115 USA
[c] Department of Mechanical Engineering, University of Connecticut, Storrs, CT 06269 USA

ARTICLE INFO

Keywords:
Shock loading
Punching
In-plane compression
Residual capacity
Failure mechanisms

ABSTRACT

Well-designed honeycomb sandwich panels are known to have superior blast performance compared to their corresponding solid panel of the same mass. However, the residual structural capacity of honeycomb sandwich panels and their blast resilience has not been systematically studied. Here, we investigate the structural behavior of all-metal honeycomb sandwich panels after shock loading using detailed numerical simulations. The initial shock is varied from relatively small intensities to moderate intensities sufficient to create material failure and significant plastic deformation in the panel. The structural response of the shock-loaded panels is investigated under quasi-static punch indentation and in-plane compression. The maximum load carrying and energy absorption capacities of shock-loaded panels are quantified for a wide range of initial shock intensities and different panel core densities. Failure maps for the honeycomb panels were constructed for each quasi-static loading condition by considering three failure modes: core failure, face sheet failure, and total panel detachment from its support. This study provides new insights into the behavior and structural resilience of the shock-loaded sandwich panels, while further highlighting their potential in the development of resilient structural systems.

1. Introduction

Critical civilian, industrial and military structures should withstand and sustain their functionality if subjected to extreme loadings (e.g. impact, blast, thermal shock, and earthquake). In this context, sandwich panels with low density core construction have shown significant promise for developing shock-resistant structures [1–18]. Xue and Hutchinson [19] showed that a sandwich panel with sufficiently strong core construction can withstand more intense blast loads and absorb more energy compared to its corresponding solid plate of the same material and mass. Extensive studies have further highlighted the superior performance of optimized sandwich panels under impulsive loadings and projectile impact [20–28] compared to traditional solid plates. Zhu and colleagues proposed a theoretical investigation to describe the mechanical response of honeycomb and aluminum foam core sandwich panels and to determine the optimal configuration of the panels [29]. They also investigated the failure behavior of honeycomb sandwich panels under both uniform and localized shock loading [30]. In recent studies, Vaziri and colleagues [31,32] investigated the performance of square honeycomb sandwich panels subjected to multiple shocks, as well as the shock impingement that is followed follows a projectile impact. The studies included development of failure maps for these complex loading scenarios in terms of loading intensities and panel geometry. There has been also a surging interest in studying blast resistance of other structural components, specially of concrete as the most used building material in infrastructure [33–38]. Yi et al. [39] experimentally evaluated the blast resistance capacity of ultra-high performance concrete to determine the possibility of using it in concrete structures and Wu et al. [40] investigated the resistance of slabs constructed with ultra-high performance concrete to a shock loading. Progressive collapse of concrete structures has been studied numerically and experimentally for structures with an initial failure due to a shock loading [41,42]. The residual strength of blast-loaded structures is one of the most important parameters to be considered in studying their blast-resistance and has been the focus of several studies to date. Luco et al. [43] compared results from static and nonlinear dynamic analyses of residual roof drift of the case-study building after blast load, and calibrated the static approach to reliably compute the residual capacity. The effect of the blast damage on the residual strength of concrete [44] and composite columns [45] was also investigated.

In this paper, we extend our previous studies on the performance of sandwich panels under high intensity dynamic loading by investigating the blast-resilience and residual structural capacity of honeycomb sandwich panels, which are shown to have excellent structural performance compared to many other core topologies [20,21,31,46]. We study the quasi-static punching and in-plane compression responses of square honeycomb sandwich panels before and after shock impingement. In view of

* Correspondence author.
E-mail address: vaziri@coe.neu.edu (A. Vaziri).

https://doi.org/10.1016/j.ijmecsci.2018.05.038
Received 22 March 2018; Received in revised form 7 May 2018; Accepted 18 May 2018
Available online 19 May 2018

extensive studies in the literature showing better performance of sandwich panels compared to the solid plate of the same mass and material [19–21,23,31,47–51], focus of the current paper will be the assessment of the resistance of shock loaded sandwich panels and comparison with corresponding solid plate will not be made. Due to the prohibitively expensive and complex nature of experimental studies on the mechanical response of structures under high intensity dynamic loading, computational techniques, specially finite element simulation, are widely used in such studies and are shown to capture with high fidelity many of the phenomenological details of the structural performance [52,53]. Finite element simulations have been validated against indentation tests performed on a foam core sandwich panel [54], and against experiments on sandwich panels with different core topologies subjected to high intensity dynamic loading, including panels with a pyramidal lattice [53,55], corrugated plate [27] and honeycomb [53,56] core constructions.

In this work, we use finite element models of the honeycomb sandwich panel developed using the commercially-available software ABAQUS (SIMULIA, Providence, RI). The model geometry and meshing are very similar to the validated computational models used in several studies [2,48], and are described in detail in Section 2. The response of the panel, including the role of panel core density and the failure map and mechanisms are discussed in Section 3 for punch indentation and in Section 4 for in-plane compression. We draw concluding remarks in Section 5.

2. Panel geometry, loading and material modeling

In this paper, we consider sandwich panels of infinite length in one direction (i.e., y-direction) and width of 2 L (in x-direction). The panel core has a height H and web spacing B, and the thicknesses of core webs and face sheets are t and h_f, respectively as shown in Fig. 1. The core relative density, ρ_c, and mass per area of the sandwich panel, M, can be derived as follows: $\rho_c = 2\frac{t}{B} - (\frac{t}{B})^2$ and $M = \rho(2h_f + \rho_c H)$, where ρ is the density of the bulk material. Following our previous studies [21,31,32,47], the web spacing, core height, and finite length of the panel are fixed at $B/H = 1$, $H/L = 0.1$, and $L = 1$ m, respectively. The mass per area of the panel is taken to be $M = 156$ kg/m^2, which is the same mass/area of a solid plate with thickness equal to 20 mm. With these parameters, the thickness of core webs and face sheets can be calculated for a given ρ_c. We only modeled one unit cell of the sandwich panel with the proper boundary conditions to represent the described geometry. As depicted in Fig. 1, clamped boundary condition is applied along the infinite edge of the model and x-symmetry condition is imposed to model only half of the panel. Since the applied loading is the same in any xz-plane, the symmetry boundary conditions in the y-faces effectively simulate periodic boundary conditions in the y-direction. The model is then meshed using eight-node hexahedral elements with reduced integration. To make sure that the model can capture early stages of necking with acceptable accuracy, at least 4 elements are employed through the thickness of each face sheet [23,47,57]. A sufficiently fine mesh was employed so that results are insensitive to element size. Core and face sheets were bonded together with the *tie* option available in ABAQUS which allows two regions to be fused together even though the created meshes on the surfaces may be dissimilar.

A moderate strength steel with low strain hardening and no strain-rate dependency, AH36 [58], is used in all the simulations. The low ductility of this steel enables our model to highlight the role of fracture limits in the response and failure of the panels. AH36 has shown to closely conform to an elasto-plastic constitutive relationship with Young's modulus $E = 200$ GPa, Poisson's ratio $\upsilon = 0.3$, yield strength $\sigma_Y = 380$ MPa and density of $\rho = 7800$ kg/m^3, with an isotropic hardening behavior that is shown in Fig. 1B [58]. We assume that when the accumulated equivalent plastic strain, which is an important internal variable in many traditional damage and fracture models [59–61], reaches a critical value, the material point fails and the element corresponding to the integration point is deleted using the scheme available in ABAQUS. The fracture strain of this steel strongly depends on the stress triaxiality (defined as the ratio of the hydrostatic mean stress, σ_m, to the von Mises equivalent stress, σ_e – See Fig. 1C) [58,62], which is taken into account in our simulations.

To model shock loading, a uniform and rapidly decaying pressure load, $\tilde{P}(t) = Pe^{-t/t_0},\ t > 0$, is applied to the top surface of the top face, where P is the peak over-pressure [20,21] and $t_0 = 10^{-4}$ s (*0.1* ms) is a typical time duration for a shock wave generated due to a blast. Fig. 1D shows the time-response of the panel with core relative density of $\rho_c = 0.04$ subjected single shock loadings with peak over-pressures $P = 30,\ 50,\ 70$ and 100 MPa. The plot shows the normalized deflection of the bottom face sheet, $\boldsymbol{\delta_{bot}/L}$ versus normalized time, $t/(\boldsymbol{L}/\sqrt{\sigma_Y/\rho})$. The deformed configuration of the panels after shock loading is also shown in Fig. 1E, where the contours correspond to the equivalent plastic deformation. For the honeycomb sandwich panel considered here, core failure is observed when $P > 100$ MPa, whereas a shock loading with $P = 130$ MPa results in total failure of the panel due to shearing off from the rigid supports. A comprehensive investigation of the failure mechanisms of sandwich panels under intense shock loading is reported in our previous work [32].

For each shock loading, we allowed the simulations to run for 10 ms before applying the quasi-static loading, to give the panel sufficient time to get into the rest position [31,32]. In punch indentation, the indenter was modeled as a rigid prismatic solid with rounded square cross section, edge length $a/L = 0.1$ and fillet radius $r/L = 0.05$. The punch was assumed to have infinite length (in y-direction) similar to the panel. Due to the contact and the very large deformations expected to occur in the simulations, the explicit solver (ABAQUS/Explicit) was chosen over the implicit solver to efficiently solve the problem. For a quasi-static simulation using the dynamic explicit solver to produce reliable results, inertia effects should be kept insignificant by ensuring that the ratio of kinetic energy to internal energy of the model does not exceed 1%. In the current work, this is achieved by limiting the punching velocity to 0.1 m/s for punch indentation and the compression rate to 0.06 m/s for in-plane compression.

3. Punch indentation of shock-loaded panels

In this section, we study the response of shock-loaded honeycomb sandwich panels under quasi-static punch indentation. Fig. 2A shows schematics of the loadings applied to the panel. Frictionless surface-to-surface contact condition is applied between the punch and the panel top face. The indentation rate is chosen to ensure a quasi-static condition (i.e., the results are independent of the indentation rate). The indentation force computed from the numerical simulations, F_{punch}, is normalized by the limit load/length F_c of a perfectly plastic solid plate of the same mass and made from the same material (i.e., $F_c = \sigma_y h^2/L$, where $h = 0.02$ m is the thickness of the solid plate [47]). The indentation force is plotted versus the displacement of punch, δ_{punch} in Fig. 2B.

3.1. Indentation force-displacement response

Fig. 2B shows the indentation responses of an intact sandwich panel (i.e. with no initial shock loading), as well as four shock-loaded sandwich panels with peak over-pressures of $P = 30,\ 50,\ 70$, and 100 MPa. The sandwich panels have a core relative density of $\rho = 0.04$ and are made of AH36 steel. For the case of an intact sandwich panel (blue line), the indentation response is initially linear up to $\delta_{punch}/L \cong 0.006$ ($F_{punch}/F_c \cong 3$), as the panel core and face sheets deform in the linear elastic regime. As the indentation displacement increases, the panel starts undergoing plastic deformation, resulting in a nonlinear response while the panel behavior gradually changes from bending- to stretching-dominated. The extensive stretching of face sheets leads to a stiffening response that is evident in the increasing indentation load by increasing indentation displacement. The indentation force reaches $F_{punch}/F_c \cong 7$ at $\delta_{punch}/L \cong 0.1$ before the bottom face sheet starts failing in the vicinity

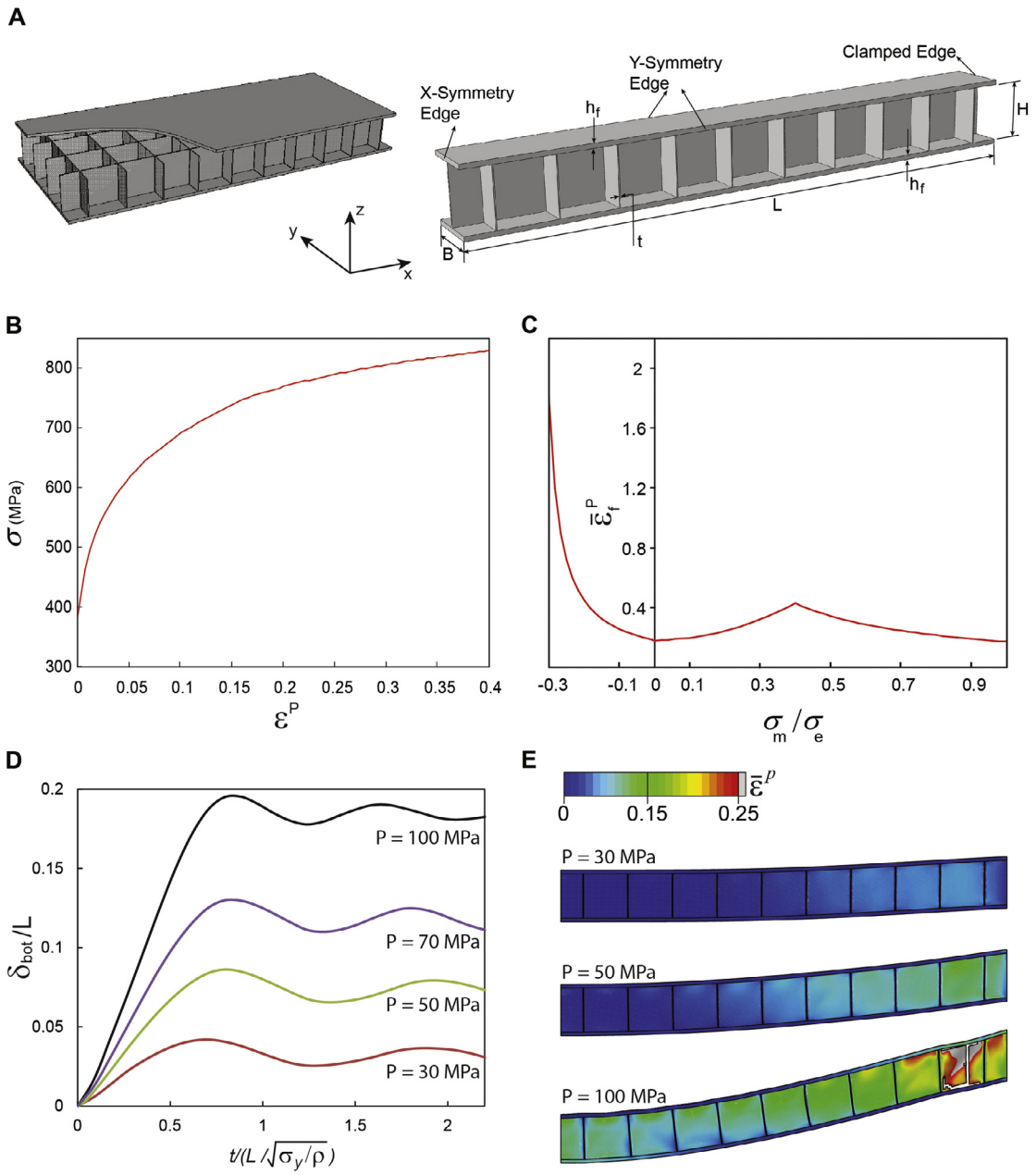

Fig. 1. (A) Schematic of square honeycomb sandwich panel and associated computational unit cell with important geometrical parameters shown. (B) True stress-true plastic strain and (C) failure locus of AH36. Failure locus shows plastic strain at failure versus stress triaxiality ratio (adopted from Lee and Wierzbicki [58]). (D) Normalized bottom face deflection of the panel with $\rho_c = 0.04$ subjected to single shock loadings of $P = 30$, 50, 70 and 100 Mpa. (E) Corresponding deformed shape of the panels after shock impingement. Contour shows plastic strain in the panel.

of the indenter (see Section 3.3 for further discussions on the failure of the panels) and the indentation force sharply drops. This is followed by a short period of stiffening behavior as the top face undergoes further stretching. Subsequently, the top face fails close to the clamped edge, resulting in another significant drop in the indentation force. At this stage, the panel core undergoes crushing and shear deformation as the indentation progresses while the indentation force remains at $F_{punch}/F_c \cong 1.5$.

The shock-loaded panels exhibit an initial force-displacement response that is near linear. This is because the initial shock loading mainly results in crushing of the core (mainly near the supports – see Fig. 1E), while the panel face sheets do not undergo significant plastic deformation (note that this is true for the range of peak over-pressures and the specific panel considered in this set of simulations except for the panel subjected to an initial shock with peak over-pressures of $P = 100$ MPa). If we define the slope of the initial near-linear response of the panels as the panel's effective stiffness, it is evident from Fig. 2B that this effective stiffness is higher for shock-loaded panels compared the intact panel. For the shock-loaded panels, the face sheet stretching has already initiated when the punch indentations starts, which results in a higher effective stiffness. The indentation force increases for all shock-loaded panels as the indentation progresses up to the point of first failure (e.g. $\delta_{punch}/L \cong 0.07$ and 0.053 for the peak over-pressures of $P = 30$ and 50 MPa, respectively) where a sudden drop in the indentation force is observed. Interestingly, the maximum indentation force in a shock-loaded panel is higher compared to a corresponding intact panel, where an initial shock with a larger peak over-pressure in the range studied here results in a higher maximum indentation force. This observation is associated with the hardening behavior of the sandwich panel material.

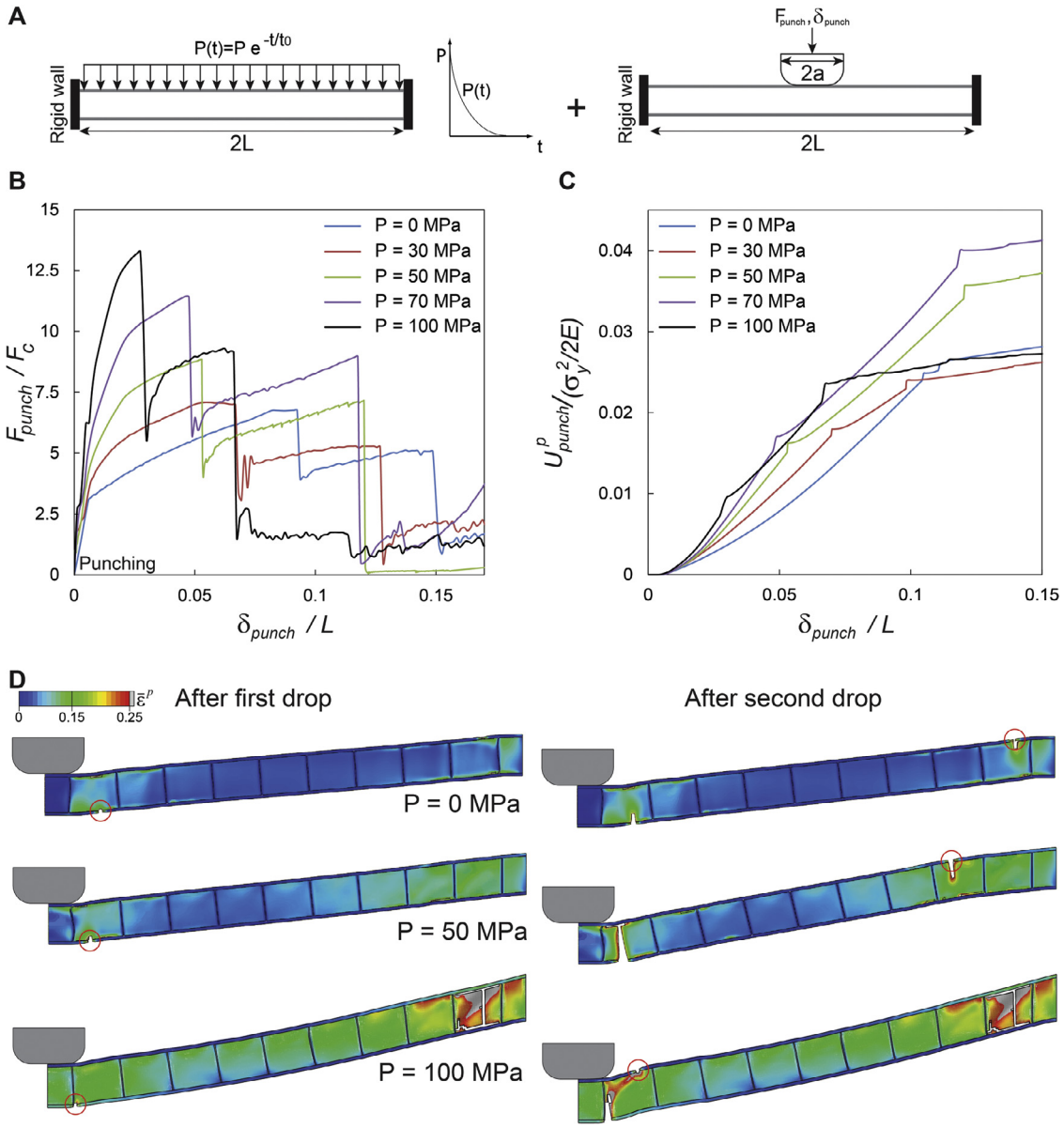

Fig. 2. (A) Schematic of a honeycomb sandwich panel subjected to a shock loading followed by quasi-static punching. (B) Normalized punching force versus indentation of the panel for three peak over-pressures of initial shock, $P=0$ (i.e. no shock) 50, and 100 Mpa. (C) Energy absorbed by the panel after shock impingement for the same panels. (D) Deformed shape of sandwich panels after first and second drops in punching force for pressure. Contours correspond to plastic strain and new failure regions in the current stage of loading are indicated by red circles. All panels have $L=1$ m, $M=156$ kg/m^2 and $\rho_c=0.04$. (For interpretation of the references to colour in this figure legend, the reader is referred to the web version of this article.)

Under the initial shock loading, the panel undergoes plastic deformation in certain areas as can be seen in Fig. 1E, which results in an increase in the maximum indentation force of the shock-loaded panel. Similar to the response of intact panels, shock-loaded panels exhibit a stiffening behavior after the initial failure. However, this stiffening behavior occurs over a larger indentation displacement compared to their corresponding intact panel, which eventually results in failure of the top face and another sudden drop in the indentation force.

The total plastic energy dissipation computed from numerical simulations is normalized by the elastic energy density of material, i.e. $\sigma_y^2/2E$, and plotted in Fig. 2C as a function of indentation displacement for all panels. The normalized energy dissipation due to the initial shock was excluded from this plot. The values of this normalized energy dissipation are 0.008, 0.025, 0.054 and 0.124 for initial shocks of $P=30$, 50, 70 and 100 MPa, respectively, as calculated using the finite element simulation. As we mentioned earlier, the early stages of indentation are in the elastic regime (for intact panels) or mostly in the elastic regime (for shock-loaded panels). As a result, there is (near-)zero plastic energy dissipation in the panels in the very early stage of indentation (i.e., $\delta_{punch}/L < 0.01$). The plastic energy dissipation increases exponentially as the indentation progresses further, with each failure incident in the panels manifesting by a small step-like increase in the dissipated energy in Fig. 2C. The total dissipated energy increases by increasing initial shock intensity except for $P=100$MPa. As it is discussed earlier, the initial shock results in plastic deformation in the panel, and consequent hardening behavior observed in the response, as well as the improvement in the energy dissipation of the panel. However, for the case of $P=100$ MPa core failure in the initial shock stage prevents it from

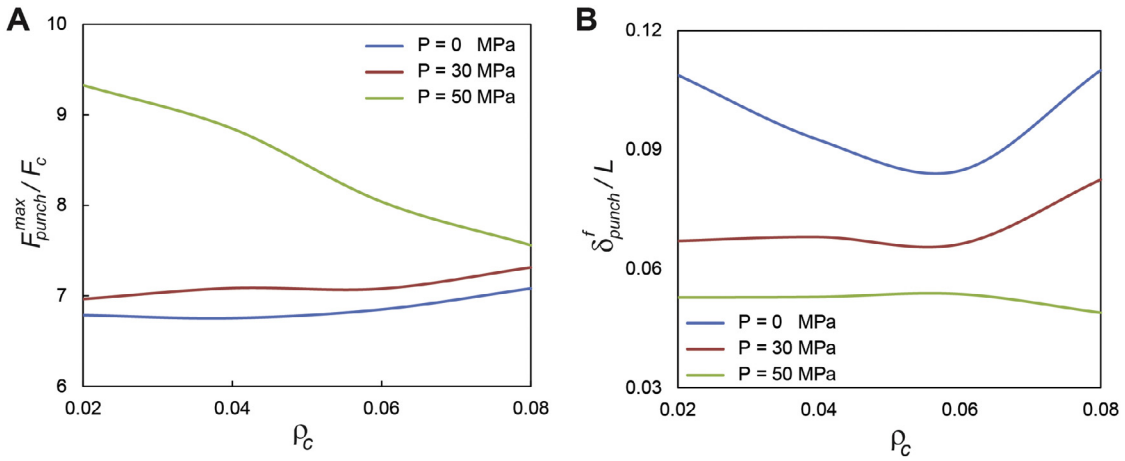

Fig. 3. (A) Normalized maximum reaction force of indenter versus core relative density of the panel for three initial shock intensities. (B) Normalized deflection at failure versus core relative density of the panel. All panels have $L = 1$ m, $M = 156$ kg/m^2.

bearing load and absorbing significant energy in the indentation stage. This figure highlights the potential of shock-loaded panels to absorb significant additional energy before losing load bearing capacity.

Fig. 2D shows the deformed configuration of the panels after the first and second significant drops in the indentation force (i.e., corresponding to the bottom and top face failures in the panel) for panels subjected to initial shock of $\boldsymbol{P} = 0$ (i.e., no shock), 50 and 100 MPa. Contours show the equivalent plastic strain in the panels, and the red circles mark failure regions. As discussed above, the first failure initiates at the bottom face sheet close to the middle of the panel, while the second failure happens in the top face sheet near the clamped boundary.

3.2. Role of core relative density

It is known that there is an optimum core relative density for square honeycomb sandwich panels for which the deflection of the panel under single shock loading [21] or multi-shock loading [31] is minimized. In this section, we aim to investigate effect of core relative density (in the range that was considered in this study, which is 0.02—0.08) on the performance of the panel in terms of maximum indentation force as well as the indentation displacement corresponding to the appearance of the first failure in the panel. In this section, we limit our study to moderate intensity shocks to better highlight the performance of the panels under indentation. Fig. 3A shows the maximum normalized indentation force (with respect to limit load $\boldsymbol{F_c}$) versus core relative density for three initial peak over-pressures, $P = 0$ (i.e. no shock), 30 and 50 MPa. The maximum indentation force occurs right before the first failure appears in the panel (i.e., first drop in the indentation force in Fig. 2B). Fig. 3A indicates that in general the shock-loaded panels resist larger indentation forces compared to an intact panel. For the initial shock of $P = 50$ MPa, the maximum indentation force decreases by increasing core relative density. As noted in the previous section, the main contribution in the indentation response comes from the face sheets of the panel as a lower core density translates to thicker face sheets, since the overall mass/area of the panels is constant. However, for the panels with minimal core deformation during the shock loading stage (i.e. $P = 0$ and 30 MPa) the indentation force is slightly higher for the panels with higher core densities, where the (near-)intact core plays a comparable role as the face sheets in the response.

The other parameter that was considered in investigating the effect of core relative density is the indentation displacement associated with the first failure of the panel, δ^f_{punch}. Fig. 3B shows the normalized indentation displacement at failure, δ^f_{punch}/L, versus the core relative density of sandwich panels for initial shock loadings of $P = 0$, 30 and 50 MPa. As mentioned in the previous section (and also discussed in the next), under quasi-static indentation face sheet failure is the first failure mode that appears in the panels subjected to an initial shock (except for $P = 100$ MPa, see Section 3.1). Therefore, the reported indentation displacements in Fig. 3B correspond to the bottom face sheet failure in the panels. The intact panels (and also the panels subjected to the lowest intensity shock, i.e. $P = 30$ MPa) with core relative densities of $\rho_c = 5 \sim 6\%$ have the minimum tolerance for face sheet failure. However, panels on the two ends of the considered range of core densities benefit from either a strong intact core structure ($\rho_c = 0.08$) or thick face sheets ($\rho_c = 0.02$) and exhibit higher indentation at failure. For the initial shock intensity of $P = 50$ MPa, the top face sheet of the panels with higher core relative densities (i.e. $\rho_c \sim 0.08$) undergoes extreme plastic bending into the core [47]. This reduces their contribution to the panel's performance and results in smaller punch indentation at failure for the panel with $\rho_c = 0.08$ when subjected to an initial shock of $P = 50$MPa.

3.3. Fracture mechanisms and failure maps

In this section we investigate failure modes and construct the failure maps of the honeycomb sandwich panels subjected to a shock loading followed by quasi-static punch indentation. Our finite element simulations revealed three failure mechanisms: (i) face sheet failure, which is defined as necking and tearing of the top or bottom face sheets; (ii) core failure, which is defined to occur when the total length of one continuous crack on the core webs exceeds the undeformed core height; and (iii) total failure of the panel, which signifies the total detachment of a panel from the support. Fig. 4A shows the failure map of a panel with core relative density of $\rho_c = 0.04$ in terms of peak over-pressure of the initial shock, and the punch indentation corresponding to the onset of each failure mode. Unlike panels subjected to a single or multiple shock loadings, where core failure is the first failure mode that appears in the panel (for example, see [21,31]), here the first sign of failure in the panel appears at the face sheets, which can be attributed to the extensive stretching of the face sheets under punch indentation rather than a uniformly distributed load (the same phenomenon can be seen in panels subjected to combined shock and projectile loading, see [32]). However, for the case of a very high intensity initial shock, i.e. $P = 100$ MPa, the shock itself initiates core failure in the panel before the indentation stage. The indentation displacement corresponding to the onset of all failure modes decreases as we increase the peak over-pressure of the shock, since the panel loses more of its capacity to carry additional load for a more intense initial shock. The decreases in indentation displacement are similar for all failure modes up to $P = 75$ MPa, after which the core failure sees a sharp decrease. For the shock intensities with $P > 75$ MPa, several material points in the core fail during the

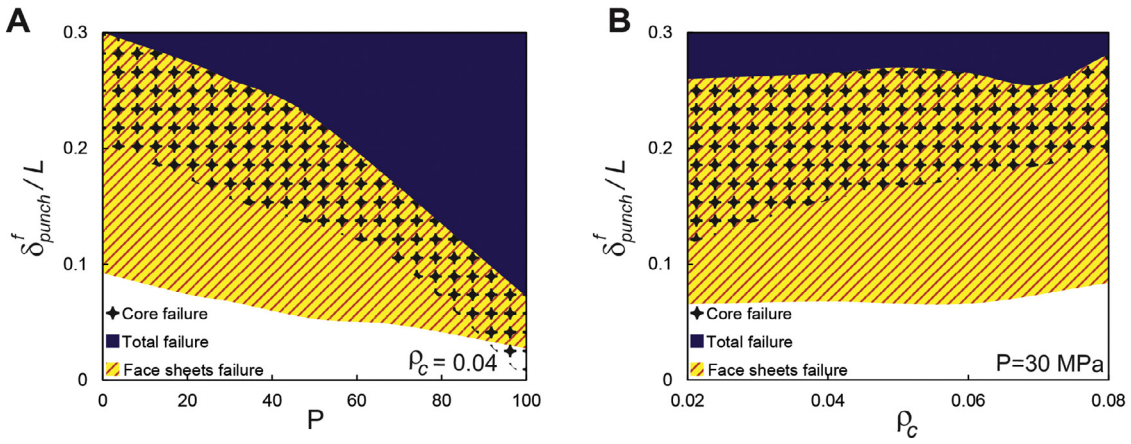

Fig. 4. Failure maps of the shock-loaded panel under quasi-static punching, identifying different mechanisms of failure. The plots show the transverse punch deflection associated with each failure mechanism versus (A) peak over-pressure of the shock applied to the panel prior to punch indentation for the panel with $\rho_c = 0.04$, and (B) core relative density of a shock-loaded panel with initial shock peak over-pressure of $P = 30$ MPa. All panels have $L = 1$ m, $M = 156$ kg/m^2.

initial shock loading (this, by definition, is not considered as core failure), which accelerates the subsequent process of core and total failure in the panel. Total failure of an intact panel, i.e., at $P = 0$ MPa, happens at $\delta^f_{punch}/L = 0.30$, while increasing peak over-pressure to $P = 100$ MPa drops this to $\delta^f_{punch}/L = 0.07$.

Next, we study the role of core relative density on the failure modes of the panel. Fig. 4B shows the failure map of the panel in terms of indentation displacement at failure and core relative density of the panels subjected to an initial shock of $P = 30$ MPa. As discussed in Fig. 3B, the indentation displacement associated with face sheet failure is smallest for panels with core densities of $\rho_c = 0.05$—0.06. Panels with lower core densities tolerate slightly higher indentations before failure due to the thicker face sheets. On the other hand, panels with higher core densities have slightly elevated indentation at failure because of the stronger (near-)intact core (note that here $P = 30$ MPa). The core failure happens at $\delta^f_{punch}/L = 0.12$ for the panel with core relative density of $\rho_c = 0.02$, and it increases with increasing core density due to the excess material in the core for panels with higher core densities. Since both face sheets and core contribute in determining the total failure of the panel, we expect the indentation displacement corresponding to total failure increase as the core density increases, hence the panel with core relative density of $\rho_c = 0.08$ resists the highest indentation before fully detachment from the support, i.e., $\delta^f_{punch}/L = 0.28$.

4. Axial compression of shock-loaded panels

Relative to out-of-plane response, the in-plane response of sandwich panels has received less attention in the literature [45,63,64], despite their promising load bearing potential in applications such as columns. The in-plane characteristics of sandwich panels has been the focus of several recent studies where the in-plane response of panels with honeycomb [65], corrugated [66] and pyramidal truss [67–69] cores was investigated experimentally, numerically and analytically. However, to date there has been no report on the compressive response of these panels after an initial shock loading. In this section we aim to investigate the performance of honeycomb sandwich panels subjected to in-plane compression after impingement of an initial shock loading. Figure 5A represents the schematic of the loading applied on the panel. The shock loading applied on the top face of the panel corresponds to a uniformly distributed pressure that exponentially decays in time. After the panel comes at a rest (i.e., after 0.1 s) an in-plane quasi-static compression applied on the right-end of the panel. A frictionless general contact formulation is employed to model contact on the panel's surfaces. We recover the compression force from the simulations and identify the failure modes.

4.1. Response of the panels

Fig. 5B shows the normalized in-plane compression force of the panel (with respect to limit load, see Section 3 for details) versus the normalized compression displacement for three different peak over-pressures of the initial shock loading with $P = 0$, 30 and 50 MPa for panels with a core relative density of $\rho_c = 0.04$. For the case of no shock (i.e. $P = 0$ MPa), the force increases linearly with the displacement until the point of shear buckling of the panel [66–69], i.e., $\delta_{comp}/L = 0.004$. Subsequently, a non-linear behavior is observed until the normalized load reaches its peak at $F_{comp}/F_c = 57$, followed by a softening post-buckling response. The stress state in the panel before shear buckling is primarily compressive. However, after this point, tensile stress and plastic deformation start to develop in the panel. This results in low stiffening behavior in the panel's response up to $\delta_{comp}/L = 0.015$. At this point, the portions of the core webs under tensile stress surpass those under compression and the compression force decreases until the core web fails in one of the core cells (defined as core failure), which is then followed by a plateau in the compression force-displacement response. The response of the shock-loaded panels under in-plane compression is initially near-linear, similar to panels subjected to punch indentation. In these panels, the initial shock deforms the panel into a sagging shape, which intuitively makes the panels' resistance to in-plane compression much lower compared than that of an intact panel. This is clear from Fig. 5B, where the effective stiffness of the panel (defined as the slope of the initial near-linear part of the response) and the maximum compression force decrease with increasing initial shock's intensity.

The dissipated plastic energy normalized by the elastic energy density of the material (i.e., $\sigma_y^2/2E$), during the compression stage is shown in Fig. 5C. The initial (near-)linear behavior of the panels is indicated by the (near-)zero plastic energy absorption in this figure. Unlike the panels under punch indentation, the plastic energy dissipated by the panel under in-plane compression is lower for the shock-loaded panels in comparison to the intact panel, and it decreases by increasing peak over-pressure of the shock. This could be attributed to the fact that under in-plane compression, only one or two cells in the core experience extensive plastic deformation and absorb plastic energy due to shear buckling of the panel. However, their energy absorption capacity is still considerable (e.g. for $P = 30$ MPa it is half of its intact equivalent), thus

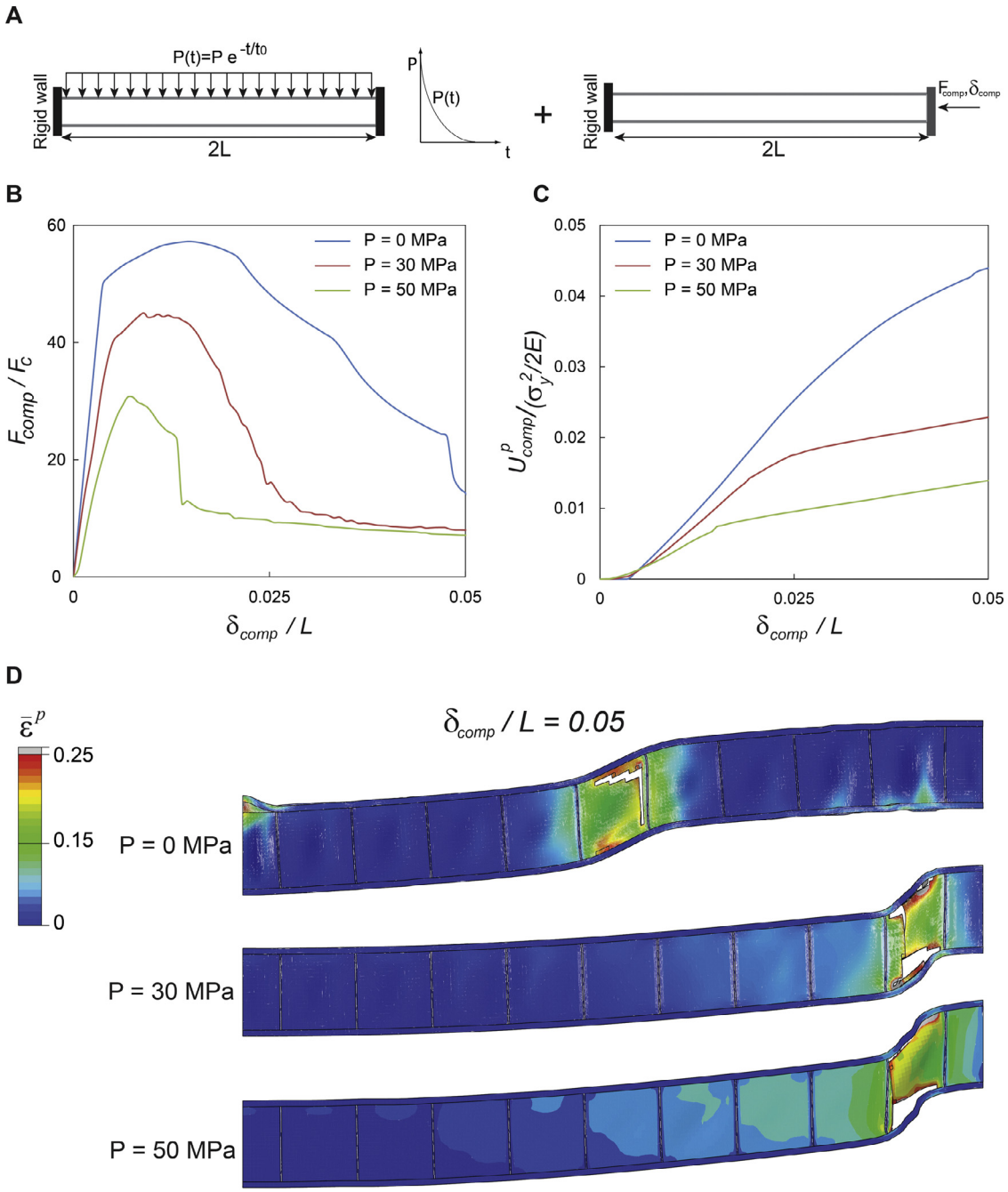

Fig. 5. (A) Schematics of honeycomb sandwich panel subject to a shock loading followed by axial compression. (B) Normalized compression force versus compression displacement of the right end of the panel after shock impingement for three peak over-pressures. (C) Normalized energy dissipation in the panel after shock impingement. (D) Deformed configuration of sandwich panels after at $\delta_{comp}/L = 0.05$. Contours correspond to plastic strain. All panels have $L = 1$ m, $M = 156$ kg/m^2 and $\rho_c = 0.04$.

these panels show great potential for developing resilient structural elements.

4.2. Role of core relative density

Changing the core relative density of a sandwich panel while keeping the total mass constant is one of the major means to modify their performance based on the application. This strategy has been shown to have a significant effect on the overall performance of the panel under different loading conditions [21,23,31,32]. This is particularly important when there is a limitation on the total mass of the structure. Here, we study the effect of the core relative density of the panel on the maximum in-plane compression force for three initial shocks with peak over-pressures of $P = 0$ (i.e., no shock), 30 and 50 MPa. Fig. 6A shows the normalized maximum compression force versus the core relative density. In the case of intact panels, both face sheets and the core have a significant contribution in determining their compression resistance. In fact, their overall bending rigidity governs their performance under in-plane compression. Increasing the core relative density decreases their overall bending rigidity, hence decreases the maximum compression force as it is clear from Fig. 6A. For the shock-loaded panels, on the other hand, the maximum compression force increases with increasing core relative density. This is due to the fact that in the already deformed panel (with a sagging shape after shock loading) the only significant resistance to

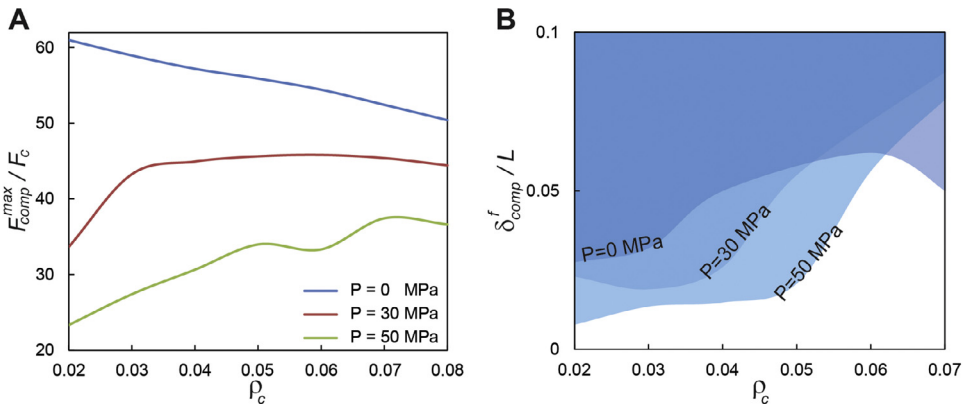

Fig. 6. (A) Normalized maximum compression force versus core relative density of the panel for three peak over-pressures of shock loading, $P = 0$, 30 and 50 Mpa. (B) Failure map of shock-loaded sandwich panel subjected to in-plane compression. Map shows compression displacement at onset of the core failure in the panel versus core relative density for three peak over-pressure of initial shock. All panels have $L = 1$ m, $M = 156$ kg/m^2.

in-plane compression comes from the shear strength of the core. Therefore, in the case of shock-loaded panels, the face sheets have a negligible effect on the compression force and the panel core is the main player in determining the maximum compression force.

4.3. Fracture mechanisms and failure maps

Fig. 6B shows the failure map of the honeycomb sandwich panels subjected to a shock loading followed by in-plane compression. In the ranges of in-plane compression and core relative density considered in this paper, core failure was the only observed failure mode. We recall that core failure is hereby defined as the length of a continuous crack in the deformed core exceeding the height of the undeformed core. The figure represents in-plane compression corresponding to core failure of the panel versus core relative density for three peak over-pressures of the initial shock. Since our simulations for the panel with $\rho_c = 0.08$ did not advance until the point of core failure, the results are plotted for panels with core density up to $\rho_c = 0.07$. In accordance with our previous discussions, a core with higher density, which is consequently stronger, withstands higher compression before failure. This trend is evident for the case of shock peak over-pressures of $P = 30$ and 50 MPa. However, for the case of no initial shock, i.e. $P = 0$ MPa, the failure onset increases by increasing core density up to $\rho_c = 0.06$, but then starts to decrease likely due to having very thin face sheets and the reduced overall bending rigidity of the panel.

5. Conclusions

We studied the performance of shock loaded all-metal honeycomb core sandwich panels in terms of their residual capacity to withstand secondary quasi-static deformation using finite element simulations. Two quasi-static loading scenarios were considered that includes quasi-static transverse punch indentation and quasi-static in-plane compression. The performance of shock loaded sandwich panels was quantified by studying their plastic energy dissipation capacity, as well as the maximum resisting force achieved prior their failure. Under punch indentation, a shock-loaded panel was shown to generally fail at a smaller indentation compared to its corresponding intact panel, while exhibiting a higher resisting force prior to failure. Our results revealed that a well-designed sandwich panel under in-plane compression can maintain up to half of its original load bearing capacity even after being exposed to a moderate intensity shock loading. We investigated the role of core relative density on the performance of honeycomb sandwich panels and constructed failure maps considering three failure modes. Based on our knowledge, this work present one of the very first studied related to blast resilience of sandwich panels, further highlighting the potential of all-metal sandwich panels in developing high performance and resilient structural systems, as well as the need for further studies on this topic (including experiments and more comprehensive parametric and optimization studies).

Acknowledgment

The authors gratefully acknowledge support by the United States National Science Foundation, Division of Civil, Mechanical, and Manufacturing Innovation, Grant No.1634560.

References

[1] Wadley H, Dharmasena K, Chen Y, Dudt P, Knight D, Charette R, Kiddy K. Compressive response of multilayered pyramidal lattices during underwater shock loading. Int J Impact Eng 2008;35:1102–14.
[2] Rathbun HJ, Radford DD, Xue Z, He MY, Yang J, Deshpande V, Fleck NA, Hutchinson JW, Zok FW, Evans AG. Performance of metallic honeycomb-core sandwich beams under shock loading. Int J Solids Struct 2006;43:1746–63.
[3] Dharmasena K, Queheillalt D, Wadley H, Chen Y, Dudt P, Knight D, Wei Z, Evans A. Dynamic response of a multilayer prismatic structure to impulsive loads incident from water. Int J Impact Eng 2009;36:632–43.
[4] Fleck NA, Deshpande VS. The resistance of clamped sandwich beams to shock loading. J Appl Mech 2004;71:386–401.
[5] Goel MD, Matsagar VA, Gupta AK. Blast resistance of stiffened sandwich panels with aluminum cenosphere syntactic foam. Int J Impact Eng 2015;77:134–46.
[6] Guan ZW, Aktas A, Potluri P, Cantwell WJ, Langdon G, Nurick GN. The blast resistance of stitched sandwich panels. Int J Impact Eng 2014;65:137–45.
[7] St-Pierre L, Fleck NA, Deshpande VS. The dynamic indentation response of sandwich panels with a corrugated or Y-frame core. Int J Mech Sci 2015;92:279–89.
[8] Yahaya MA, Ruan D, Lu G, Dargusch MS. Response of aluminium honeycomb sandwich panels subjected to foam projectile impact – An experimental study. Int J Impact Eng 2015;75:100–9.
[9] Langdon GS, Karagiozova D, von Klemperer CJ, Nurick GN, Ozinsky A, Pickering EG. The air-blast response of sandwich panels with composite face sheets and polymer foam cores: experiments and predictions. Int J Impact Eng 2013;54:64–82.
[10] Xiong J, Mines R, Ghosh R, Vaziri A, Ma L, Ohrndorf A, Christ H-J, Wu L. Advanced micro-lattice materials. Adv Eng Mater 2015;17:1253–64.
[11] Li S, Li X, Wang Z, Wu G, Lu G, Zhao L. Sandwich panels with layered graded aluminum honeycomb cores under blast loading. Compos Struct 2017;173:242–54.
[12] Rolfe E, Kelly M, Arora H, Hooper PA, Dear JP. Failure analysis using X-ray computed tomography of composite sandwich panels subjected to full-scale blast loading. Compos Part B 2017;129:26–40.
[13] Kelly M, Arora H, Worley A, Kaye M, Linz PD, Hooper PA, Dear JP. Sandwich panel cores for blast applications: materials and graded density. Exp Mech 2016;56:523–44.
[14] Ahmed S, Galal K. Effectiveness of FRP sandwich panels for blast resistance. Compos Struct 2017;163:454–64.
[15] Imbalzano G, Linforth S, Ngo TD, Lee PVS, Tran P. Blast resistance of auxetic and honeycomb sandwich panels: comparisons and parametric designs. Compos Struct 2017.
[16] Arora H, Hooper P, Linz P, Yang H, Dear J. Modelling the behaviour of composite sandwich structures when subject to air-blast loading, 2016, 6 (2016).
[17] Fan Z, Liu Y, Xu P. Blast resistance of metallic sandwich panels subjected to proximity underwater explosion. Int J Impact Eng 2016;93:128–35.

[18] Zhang P, Cheng Y, Liu J, Li Y, Zhang C, Hou H, Wang C. Experimental study on the dynamic response of foam-filled corrugated core sandwich panels subjected to air blast loading. Compos Part B 2016;105:67–81.
[19] Xue Z, Hutchinson JW. Preliminary assessment of sandwich plates subject to blast loads. Int J Mech Sci 2003;45:687–705.
[20] Vaziri A, Hutchinson JW. Metal sandwich plates subject to intense air shocks. Int J Solids Struct 2007;44:2021–35.
[21] Vaziri A, Xue Z, Hutchinson JW. Performance and failure of metal sandwich plates subject to shock loading. J Mech Mat 2007;2:1947–64.
[22] Wadley H, Dharmasena K, Queheillalt D, Chen YC, Dudt P, Knight D, Xue Z, Vaziri A. Dynamic crushing of square honeycomb structures during underwater impulsive loading. J Mech Mater Struct 2007;2:2025–48.
[23] Xue Z, Hutchinson JW. A comparative study of impulse-resistant metal sandwich plates. Int J Impact Eng 2004;30:1283–305.
[24] Lin C, Fatt MSH. Perforation of composite plates and sandwich panels under quasi-static and projectile loading. J Compos Mater 2006;40:1801–40.
[25] Liang Y, Spuskanyuk AV, Flores SE, Hayhurst DR, Hutchinson JW, McMeeking RM, Evans AG. The response of metallic sandwich panels to water blast. J Appl Mech 2005;74:81–99.
[26] Wei Z, Deshpande VS, Evans AG, Dharmasena KP, Queheillalt DT, Wadley HNG, Murty YV, Elzey RK, Dudt P, Chen Y, Knight D, Kiddy K. The resistance of metallic plates to localized impulse. J Mech Phys Solids 2008;56:2074–91.
[27] Li X, Wang Z, Zhu F, Wu G, Zhao L. Response of aluminium corrugated sandwich panels under air blast loadings: experiment and numerical simulation. Int J Impact Eng 2014;65:79–88.
[28] Wadley HNG, Børvik T, Olovsson L, Wetzel JJ, Dharmasena KP, Hopperstad OS, Deshpande VS, Hutchinson JW. Deformation and fracture of impulsively loaded sandwich panels. J Mech Phys Solids 2013;61:674–99.
[29] Zhu F, Wang Z, Lu G, Zhao L. Analytical investigation and optimal design of sandwich panels subjected to shock loading. Mater Des 2009;30:91–100.
[30] Zhu F, Lu G, Ruan D, Shu D. Tearing of metallic sandwich panels subjected to air shock loading. Struct Eng Mech 2009;32:351–70.
[31] Ebrahimi H, Vaziri A. Metallic sandwich panels subjected to multiple intense shocks. Int J Solids Struct 2013;50:1164–76.
[32] Ebrahimi H, Ghosh R, Mahdi E, Nayeb-Hashemi H, Vaziri A. Honeycomb sandwich panels subjected to combined shock and projectile impact. Int J Impact Eng 2016;95:1–11.
[33] Shi Y, Li Z-X, Hao H. A new method for progressive collapse analysis of RC frames under blast loading. Eng Struct 2010;32:1691–703.
[34] Almusallam T, Elsanadedy H, Abbas H, Alsayed S, Al-Salloum Y. Progressive collapse analysis of a RC building subjected to blast loads. Struct Eng Mech 2010;36:301–19.
[35] Millard S, Molyneaux T, Barnett S, Gao X. Dynamic enhancement of blast-resistant ultra high performance fibre-reinforced concrete under flexural and shear loading. Int J Impact Eng 2010;37:405–13.
[36] Aoude H, Dagenais FP, Burrell RP, Saatcioglu M. Behavior of ultra-high performance fiber reinforced concrete columns under blast loading. Int J Impact Eng 2015;80:185–202.
[37] Li J, Wu C, Hao H. An experimental and numerical study of reinforced ultra-high performance concrete slabs under blast loads. Mater Des 2015;82:64–76.
[38] Krauthammer T. Blast-resistant structural concrete and steel connections. Int J Impact Eng 1999;22:887–910.
[39] Yi N-H, Kim J-HJ, Han T-S, Cho Y-G, Lee JH. Blast-resistant characteristics of ultra-high strength concrete and reactive powder concrete. Constr Build Mater 2012;28:694–707.
[40] Wu C, Oehlers DJ, Rebentrost M, Leach J, Whittaker AS. Blast testing of ultra-high performance fibre and FRP-retrofitted concrete slabs. Eng Struct 2009;31:2060–9.
[41] Sasani M. Progressive collapse resistance of reinforced concrete structures. In: Shukla A, Rajapakse YDS, Hynes ME, editors. Blast mitigation: experimental and numerical studies. New York, New York, NY: Springer; 2014. p. 331–50.
[42] Keyvani L, Sasani M. Analytical and experimental evaluation of progressive collapse resistance of a flat-slab posttensioned parking garage. J Struct Eng 2015;141 04015030.
[43] Luco N, Bazzurro P, Cornell CA. Dynamic versus static computation of the residual capacity of a mainshock-damaged building to withstand an aftershock. 13th world conference on earthquake engineering; 2004.
[44] Bao X, Li B. Residual strength of blast damaged reinforced concrete columns. Int J Impact Eng 2010;37:295–308.
[45] Wu K-C, Li B, Tsai K-C. The effects of explosive mass ratio on residual compressive capacity of contact blast damaged composite columns. J Constr Steel Res 2011;67:602–12.
[46] Wadley HNG, Fleck NA, Evans AG. Fabrication and structural performance of periodic cellular metal sandwich structures. Compos Sci Technol 2003;63:2331–43.
[47] Vaziri A, Xue Z, Hutchinson JW. Metal sandwich plates with polymeric foam-filled cores. J Mech Mater Struct 2006;1:95–128.
[48] Dharmasena KP, Wadley HNG, Xue Z, Hutchinson JW. Mechanical response of metallic honeycomb sandwich panel structures to high-intensity dynamic loading. Int J Impact Eng 2008;35:1063–74.
[49] Rimoli JJ, Talamini B, Wetzel JJ, Dharmasena KP, Radovitzky R, Wadley HNG. Wet-sand impulse loading of metallic plates and corrugated core sandwich panels. Int J Impact Eng 2011;38:837–48.
[50] Dharmasena KP, Wadley HNG, Williams K, Xue Z, Hutchinson JW. Response of metallic pyramidal lattice core sandwich panels to high intensity impulsive loading in air. Int J Impact Eng 2011;38:275–89.
[51] Karagiozova D, Nurick GN, Langdon GS. Behaviour of sandwich panels subject to intense air blasts – Part 2: numerical simulation. Compos Struct 2009;91:442–50.
[52] Mohr D, Xue Z, Vaziri A. Quasi-static punch indentation of a honeycomb sandwich plate: experiments and constitutive modeling. J Mech Mater Struct 2006;1:581–604.
[53] Mori LF, Lee S, Xue ZY, Vaziri A, Queheillalt DT, Dharmasena KP, Wadley HNG, Hutchinson JW, Espinosa HD. Deformation and fracture modes of sandwich structures subjected to underwater impulsive loads. J Mech Mater Struct 2007;2:26.
[54] Rizov V, Shipsha A, Zenkert D. Indentation study of foam core sandwich composite panels. Compos Struct 2005;69:95–102.
[55] Wei Z, Dharmasena KP, Wadley HNG, Evans AG. Analysis and interpretation of a test for characterizing the response of sandwich panels to water blast. Int J Impact Eng 2007;34:1602–18.
[56] Zhu F, Zhao L, Lu G, Gad E. A numerical simulation of the blast impact of square metallic sandwich panels. Int J Impact Eng 2009;36:687–99.
[57] Xue Z, Vaziri A, Hutchinson JW. Non-uniform constitutive model for compressible orthotropic materials with application to sandwich plate cores. Comput Model Eng Sci 2005;10:79–95.
[58] Lee Y-W, Wierzbicki T. Fracture prediction of thin plates under localized impulsive loading. Part II: discing and petalling. Int J Impact Eng 2005;31:1277–308.
[59] Johnson GR, Cook WH. A constitutive model and data for metals subjected to large strains, high strain rates and high temperatures. In: Proceeding of 7th international symposium on ballistics; 1983. p. 7.
[60] Lemaitre J. A Continuous damage mechanics model for ductile fracture. J Eng Mater Technol 1985;107:83–9.
[61] Bao Y, Wierzbicki T. On fracture locus in the equivalent strain and stress triaxiality space. Int J Mech Sci 2004;46:81–98.
[62] Lee Y-W, Woertz JC, Wierzbicki T. Fracture prediction of thin plates under hemi–spherical punch with calibration and experimental verification. Int J Mech Sci 2004;46:751–81.
[63] Fleck N, Sridhar I. End compression of sandwich columns. Compos Part A 2002;33:353–9.
[64] Gdoutos EE, Daniel IM, Wang KA. Compression facing wrinkling of composite sandwich structures. Mech Mater 2003;35:511–22.
[65] Xiong J, Zhang M, Stocchi A, Hu H, Ma L, Wu L, Zhang Z. Mechanical behaviors of carbon fiber composite sandwich columns with three dimensional honeycomb cores under in-plane compression. Compos Part B 2014;60:350–8.
[66] Biagi R, Bart-Smith H. In-plane column response of metallic corrugated core sandwich panels. Int J Solids Struct 2012;49:3901–14.
[67] Cote F, Biagi R, Bart-Smith H, Deshpande VS. Structural response of pyramidal core sandwich columns. Int J Solids Struct 2007;44:3533–56.
[68] Li M, Wu L, Ma L, Wang B, Guan Z. Structural response of all-composite pyramidal truss core sandwich columns in end compression. Compos Struct 2011;93:1964–72.
[69] Xiong J, Ma L, Wu L, Liu J, Vaziri A. Mechanical behavior and failure of composite pyramidal truss core sandwich columns. Compos Part B 2011;42:938–45.